ACS Sustainable Chemistry & Engineering

Research Article

pubs.acs.org/journal/ascecg

Preparation of Si/Sn-Based Nanoparticles Composited with Carbon Fibers and Improved Electrochemical Performance as Anode Materials

Haiying Wang,[†] Hongqin Huang,[†] Lin Chen,[†] Chunguang Wang,[†] Bo Yan,[†] Yongtao Yu,[‡] Yang Yang,*[,†] and Gang Yang*[,†]

[†]Jiangsu Laboratory of Advanced Functional Material, Department of Chemistry, Changshu Institute of Technology, Changshu 215500, China

[‡]Petrochina Jilin, Petrochemical Company Research Institution, Jilin 132021, China

ABSTRACT: Si/Sn-based nanoparticles with various particle sizes are enwrapped in carbon nanofibers to improve the stability of Si/Sn during lithium alloying and dealloying. The composite structure of Si/Sn@carbon fibers is controllably synthesized by electrospinning and heat treatment. The crystal structure, content, and morphologies of Si/Sn@carbon composites are tunable by the carbonization conditions. The electrochemical performance of the composites is improved by the buffer effect of carbon fibers. The sample of SiSnC_800, which the precursor TEOS/$SnCl_2$/PAN, is carbonized at 800 °C, delivers a specific capacity of 1347 mAh g^{-1} at the second cycles, and retains 1073 mAh g^{-1} at 50th cycle. The as-synthesized samples are flexible self-supporting films, which can be directly used as anode materials for lithium ion batteries.

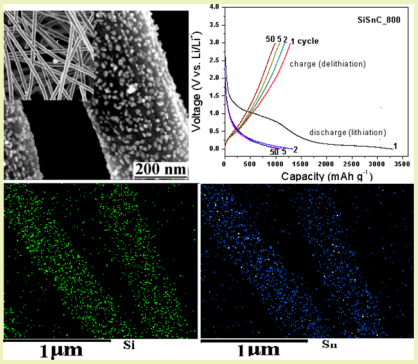

KEYWORDS: *Lithium ion batteries, Anode materials, Si/Sn@carbon, Composite materials, Electrospinning*

INTRODUCTION

Nowadays, rechargeable lithium ion batteries (LIBs) are the most important power sources for clean energy. Graphite materials, as anode electrodes, provide excellent behavior during continuous charge/discharge cycles. However, the low theoretical capacity (372 mAh g^{-1}) hardly meets the demands of high energy densities, safety, and long cyclic life in electrical vehicles (EV) and energy storage devices, etc.[1−4] Researches on alternative anodes are therefore focused on materials of higher lithium storage capacities. Among the candidates, alloy anodes such as silicon (Si) and tin (Sn) have attracted great attention because of their advantages of high performance, low cost, and low toxicity in the environment.[5−7] Tin and silicon can form alloys with lithium to store energy of 994 and 4200 $mAhg^{-1}$, respectively, providing much higher capacities than obtained from carbon. However, volume changes and the aggregation of metal take place during lithium alloying/dealloying. For example, lithiation with Si and Sn experiences volume expansions beyond 300%.[11] Because the volume change always results in mechanical breakage and poor electrical contact between the electrode and current collector, big capacity fading during charge/discharge cycles limits the wide application of metallic silicon and tin materials as anode materials for LIBs.[8−12]

To resolve the disadvantages of metallic anodes, many researchers have focused on the synthesis of metal alloys with less active or inactive metal elements, such as Fe/Si, Co/Si, Ni/Sn, and Sn/Ag,[13−20] to relax volume expansion during lithium alloying. However, the active/inactive composite systems result in either large irreversible losses or capacity fade.[13−20] By comparison, Si/Sn and Si/Sn/Sb multimetal composites present good electrochemical properties to decrease the volume change of the electrode during charge/discharge.[21−28]

Another effective approach is the active component of metal composited with porous carbon. The electrode performance can be successfully improved because the electrically conductive porous carbon provides a suitable matrix for nanostructured active grains to undergo lithium alloying and dealloying with a minimal volume change and capacity loss.[29−33] For example, Si/C and Sn/C composites with highly dispersed metal nanoparticles in porous carbon minimize mechanical stress during lithiation and delithiation. Zhou et al. synthesized silicon nanoparticles coated by carbon. The carbon shell provides voids to decrease the volume change during silicon lithiation/delithiation, and their sample delivers 617.7 mAh g^{-1} beyond 20 cycles.[31] Jung et al. reported Sn/carbon with a core−shell structure produced through microemulsion polymerization retained about 360 mAh g^{-1} after 20 cycles.[32] Zou et al. prepared a Sn/carbon film, which delivered 382 mAh g^{-1} at the 20th cycle.[33]

Electrospinning as a facile method to synthesize one-dimensional (1-D) porous carbon has been wildly utilized in

Received: May 3, 2014
Revised: August 26, 2014
Published: August 28, 2014

the preparation of 1-D nanomaterials.[34−37] After heat treatment in a nitrogen atmosphere, the polymers such as PAN and PVP convert to 1-D porous carbon fibers.[38−41] Carbon fiber provides an efficient buffering zone to decrease the volume change of metal during lithium alloying and dealloying, and thus, the metal@carbon fiber could present enhanced electrochemical performance as an anode material for LIBs. In previous publications, the composite of MnO_x and tin nanoparticles co-enwrapped in carbon nanofibers were synthesized by electrospinning and heat treatment, which shows improved electrochemical performance, especially cyclic ability.[42,43] To our best knowledge, the previous work did not describe the compositing morphology of the Si/Sn nanoparticles dispersed in carbon nanofibers and the relative electrochemical performance. The Si/Sn@carbon multimetal composite is a potential anode material for high performance LIBs. First, Si and Sn anodes with high intrinsic theoretical capacities after being combined in a composite retain a high capacity because metallic Sn with good conductivity also plays the role of conductivity aid for the anode of Si.[22] Second, the homogeneously dispersed conductive Sn nanoparticles yield a highly conductive nonwoven film.[44] Third, Sn has the ability to coat Si nanoparticles and reduce the interaction of Si with carbon because SiC is inactive and results in capacity loss.[45]

In this work, a series of nanocomposites of Si/Sn nanoparticles enwrapped in porous carbon fibers are synthesized by electrospinning and heat treatment. The diameters of the carbon fibers and the configuration of the enwrapped Si/Sn nanoparticles are carefully controlled by carbonization temperature. The compositions and morphologies of the samples are characterized by X-ray diffraction patterns (XRD), field emission scanning electron microscopy and energy dispersive X-ray detectors (FE-SEM and EDX, SIGMA, ZEISS), and Fourier transform-infrared spectroscopy (FT-IR) analysis. The as-synthesized samples are evaluated as anode materials for LIBs in detail.

EXPERIMENTAL SECTION

Preparation of TEOS/$SnCl_2$/PAN Film. Polyacrylonitrile (PAN, M_w = 150,000), tetraethoxysilane (TEOS), and stannic chloride ($SnCl_2$, 98%) were analytical reagents. Dimethylformamide (DMF) was the solvent. PAN was dissolved and stirred in DMF for 12 h to produce a 10 wt % solution. A total of 0.5 g of TEOS and 0.5 g of $SnCl_2$ was slowly added to 10 g of the solution of PAN, and the mixture was stirred for 6 h. The solution was held in a spinning nozzle with a tip diameter of 1 mm. The working high voltage is 20 kV, and the distance between the needle and collector is 12 cm in the electrospinning system. After electrospinning, a white-colored film containing Sn/Sn was removed and obtained from the aluminum collector.

Synthesis of Si/Sn@carbon Nanofibers. TEOS/$SnCl_2$/PAN film was heated at 250 °C for 1 h to increase the stability of PAN, accompanying the color change. The black film is subsequently heated in a N_2 atmosphere at 500, 700, and 800 °C for 3 h, and the products are simply termed as SiSnC_500, SiSnC_700, and SiSnC_800, respectively.

Characterization. XRD patterns are collected at a 0.02° step width from 10° to 80° (Rigaku diffractometer, Cu K_α radiation). The products are measured by using a field emission scanning electron microscope and energy dispersive X-ray detector (FE-SEM and EDX, SIGMA, ZEISS), FT-IR spectra (BRUKER VECTOR 22 spectrometer), X-ray photoelectron spectra (XPS, ESCLAB MKII), and Raman spectra (Renishaw system 1000 spectrometer with air-cooled CCD detector).

Electrochemical Analysis. Electrochemical charge/discharge tests are evaluated in CR2016 coin cells. The Si/Sn@C nanofibers were directly used as anodes without binder or conductive additive. Lithium foil was the counter electrode. A Celgard 2300 porous membrane was the separator, and 1 M $LiPF_6$ in EC: DMC (1:1) was the electrolyte. The cell was a charge/discharge under a current density of 420 mA g^{-1} between 0 and 3.0 V vs Li/Li^+.

RESULTS AND DISCUSSION

The manufacture of metal/carbon fibers from the precursors of metal salt/PAN fibers includes two steps: thermal stabilization and carbonization of PAN matrix. The first step, stabilization of PAN, involves the heat treatment of TEOS/$SnCl_2$/PAN fibers under 250 °C in air. PAN molecules undergo physical and chemical changes because PAN linear molecular chains convert to an aromatic ladder structure, which is suitable for further carbonization and conversion to carbon fibers. The oxidation and cyclozation of PAN molecules after heat treatment effectively avoid the decomposing of PAN under high-temperature carbonization. TEOS and $SnCl_2$ are simultaneously oxidized during the cyclozation of PAN molecules. In the following carbonization process, the polymer of PAN converts to carbon fiber, while silicon and tin crystals are produced because partial SiO_2 and SnO_2 has been reduced by carbon.

The FT-IR spectra of the samples are shown in Figure 1. Before heat treatment, −CN and −NH stretching vibrations in

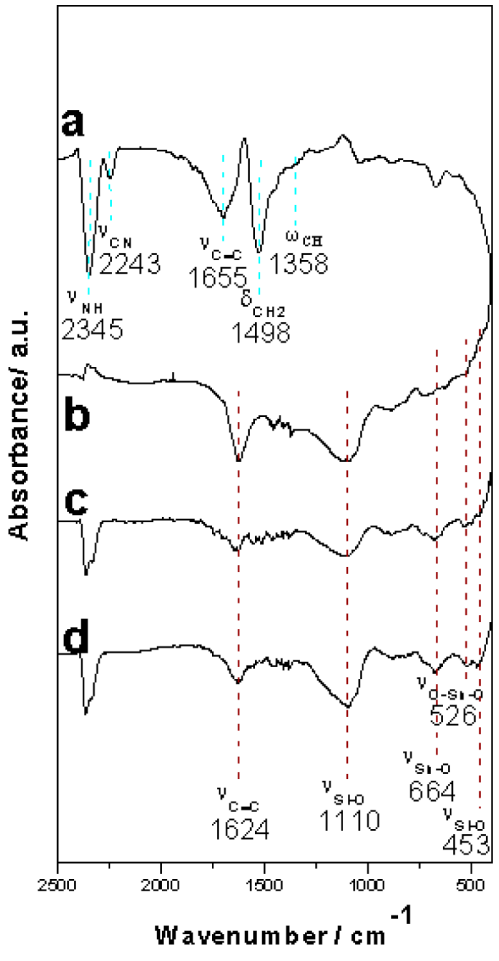

Figure 1. FT-IR spectra of (a) the sample before heat treatment, (b) SiSnC_500, (c) SiSnC_700, and (d) SiSnC_800.

PAN chains appear as absorption peaks at 2243 and 2345 cm^{-1}, respectively. The bands of 1498 and 1358 cm^{-1} are assigned to the vibrations of δ_{C-H} in CH_2 and ω_{C-H} in CH, respectively. The absorption at 1655 cm^{-1} may be attributed to the stretching C−C.[28] After heat treatment at 500, 700, and 800 °C, the spectra indicated that a −CN band and −NH band disappeared. Because of the cyclozation and dehydrogenation of PAN, the peak at 1655 cm^{-1} assigned to the C−C stretching vibration shifts to 1624 cm^{-1}, which reveals PAN fiber converted to carbon.[46] There are several weak peaks around 1110 and 453 cm^{-1} attributed to the vibration of Si−O and the new peaks around 664 and 526 cm^{-1} attributed to the vibrations of Sn−O and O−Sn−O, respectively, indicating the presence of SiO_2 and SnO_2.

Figure 2 shows the SEM images of SiSnC_500, SiSnC_700, and SiSnC_800 nanofibers. The nanofibers are uniform and

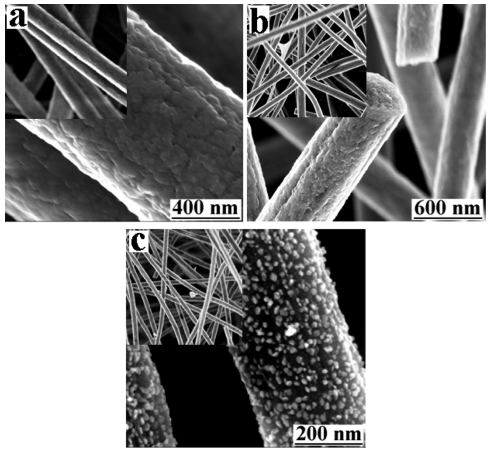

Figure 2. SEM images of (a) SiSnC_500, (b) SiSnC_700, and (c) SiSnC_800.

without the presence of any beads. The diameters of the nanofibers are dependent on the heat treatment temperatures. After the H, N, and O elements are removed from PAN and partial carbon is involved in the reduction of tin oxide at high temperature, the diameters of the Sn@C fibers are decreased. Along with the increased heat treatment temperature from 500 and 700 to 800 °C, the average diameter of the fiber was reduced from 800 and 600 to 400 nm, respectively.

The XRD patterns and the compositions of the as-synthesized Si/Sn@C nanofibers are shown in Figure 3. The component of the sample is strongly dependent on the heat treatment temperature. At the lowest temperature of 500 °C, the peaks of SiSn_500 are assigned to Si (JCPDS No. 01-0787), graphite (JCPDS No. 03-0401), and SnO (JCPDS No. 13-0111). The phase of Sn cannot be observed because tin oxide is hardly reduced at low temperature.[47] The broad peak around 23° indicates the presence of amorphous SiO_2 and carbon. Increasing the heat treatment temperature to 700 °C, mixed diffraction patterns of Si, graphite, SnO, and metallic Sn (JCPDS No. 04-0673) are present. At the highest carbonization temperature of 800 °C, the reflection lines of the sample mainly correspond to the phases of SiO_2, Si, and graphite. The phase of crystalline Sn cannot be observed, which might be because the Sn phase is amorphous.[48,49] EDX spectra of samples SiSnC_500, SiSnC_700, and SiSnC_800 are shown in Figure 3b−d. The presence of C, O, Si, and Sn corresponds to C, Si, Sn, SiO_2, and SnO_2, respectively, and no other distinguishable impurity peaks occurred. Elemental mapping images (Figure 4) clearly present Si and Sn elements evenly spread over the entire area of the nanofiber.

To investigate the vibrational properties of the SiSnC samples carbonized at various temperatures, the characterization of Raman spectroscopy has been performed, and Figure 5 shows the Raman spectra of SiSnC_500, SiSnC_700, and SiSnC_800. The peaks at 1590 and 1357 cm^{-1} are attributed to the Raman-active E_{2g} in-plane vibration mode and the Raman-inactive A_{1g} in-plane breathing vibration mode, which are named G- (graphite) and D- (disorder) bands, respectively. The *R*-value calculated by the relative intensity ratios of the D- to G-bands reflects the degree of graphitization and alignment of the graphitic plane. Lower *R*-values correspond to higher amounts of sp^2 (graphite) clusters.[50] In this work, SiSnC_500, SiSnC_700, and SiSnC_800 have *R* values of 1.049, 1.025, and 0.983, respectively, much lower than that of the pure carbon nanofibers (CNFs) reported before (I_D/I_G = 1.20).[51]

The XPS spectra of Si 2p are compared in Figure 6, in which the peaks at 99.6 and 102.8 eV correspond Si−C and Si−N−O bonds, respectively.[52,53] With an increase in heat treatment temperature from 500 and 700 to 800 °C, the relative intensity of the Si−C peak increased. The Sn spectrum of XPS consists of two spin−orbit peaks Sn $3d_{3/2}$ and Sn $3d_{5/2}$ located at 495.6 and 487.2 eV, respectively. The position of the Sn $3d_{5/2}$ peak agrees with that reported for the Sn−O bond in which Sn is in the tetravalent oxidation state as in SnO.[54] With an increase in heat treatment temperature at 700 and 800 °C, the two peaks at 493.7 and 485.2 eV are attribute to the presence of metallic Sn.[55] As shown in Figure 6, the XPS spectra of C 1s indicates the binding energies of the three different functional groups: C−C (284.8 eV), C−O (286.4 eV), and C−O−H (288.9 eV), respectively. Upon carbothermal reduction, a significant decline in the peak intensities corresponding to C−O and C−O−H can be observed with an analogous increase in intensity of the C−C peak at 284.8 eV, which clearly indicates that the quality of graphite increased.[56]

The charge/discharge curves and cyclic performance of SiSnC_500, SiSnC_700, and SiSnC_800 are shown in Figure 7. The voltage plateau in the range of 3−0.8 V comes from the growth of the solid electrolyte interface (SEI) on the electrode, which consumes large amounts of Li ions. The voltage slope between 0.8 and 0.35 V corresponds to the electrochemical reaction between Li and Sn. The long potential plateau of 0.2 V is assigned to the insertion of Li ions in the Si-based anode material to form Li_xSi alloys because SiO_2 nanoparticles are involved in the lithiation/delithiation and provide capacities.[57] There are big irreversible capacity losses in the first cycle, which mainly come from SEI and the irreversible phase transformation of metallic anodes.[58] In the second cycle, the irreversible capacity loss is rapidly decreased, and the Coulombic efficiency of the composite electrode increases close to 100%. As shown in Figure 7, the three samples show the relationship between the capacities and the preparation temperatures of the composites. For example, the samples of SiSnC_500, SiSnC_700, and SiSnC_800 deliver the initial discharge capacity of 593.4, 1490.1, and 3313.2 $mAhg^{-1}$, respectively. Sample SiSnC_800 presents a higher initial discharge capacity than SiSnC_500 and SiSnC_700. Moreover, the second cycle of Coulombic efficiency (68%) of the SiSnC_500 electrode is much lower than those of SiSnC_700 and SiSn_800. The samples of SiSnC_700 and SiSnC_800 present relatively higher initial Coulombic

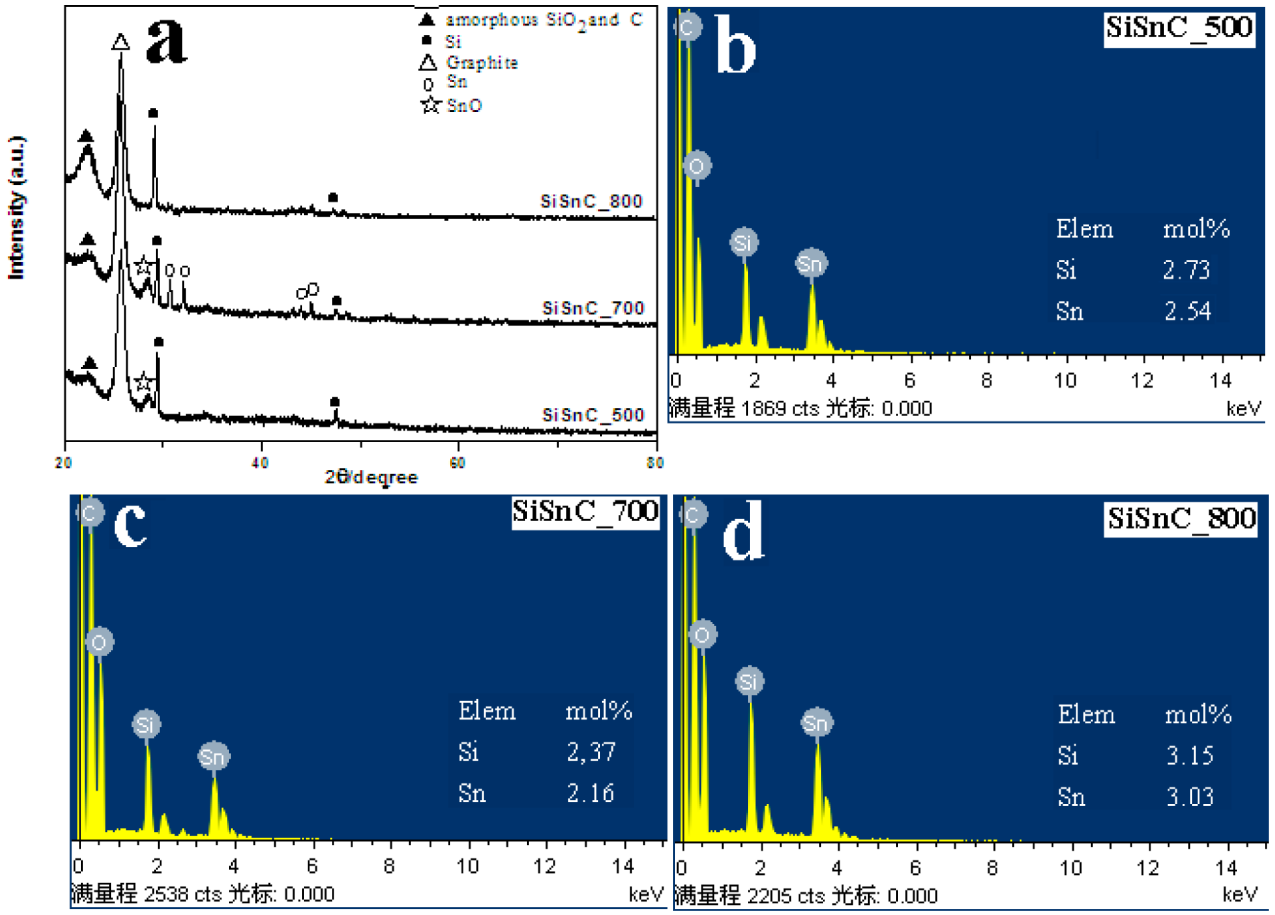

Figure 3. XRD (a) and EDX spectra of (b) SiSnC_500, (c) SiSnC_700, and (d) SiSnC_800.

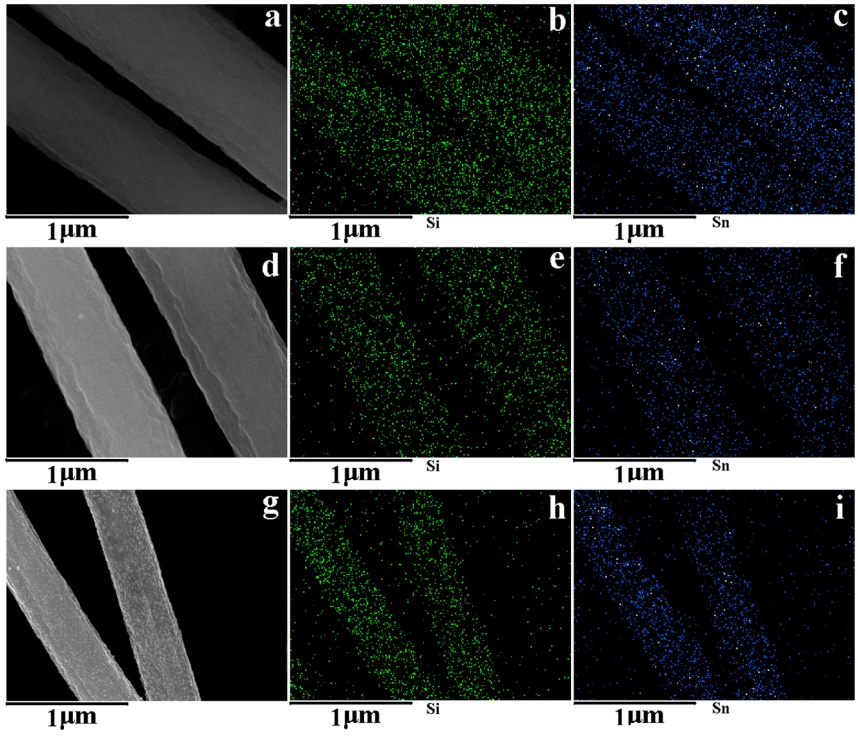

Figure 4. SEM images and elemental mapping of Si and Sn: (a–c) SiSnC_500, (d–f) SiSnC_700, and (g–i) SiSnC_800.

efficiencies of 94% and 95%, respectively. Sample SiSnC_800, where Si and Sn nanoparticles are properly dispersed in carbon fibers, delivers the capacity of 1347 mAh g^{-1} at the second cycle and retains a capacity of 1073 mAh g^{-1} after 50 cycles. The

dx.doi.org/10.1021/sc500290x | ACS Sustainable Chem. Eng. 2014, 2, 2310–2317

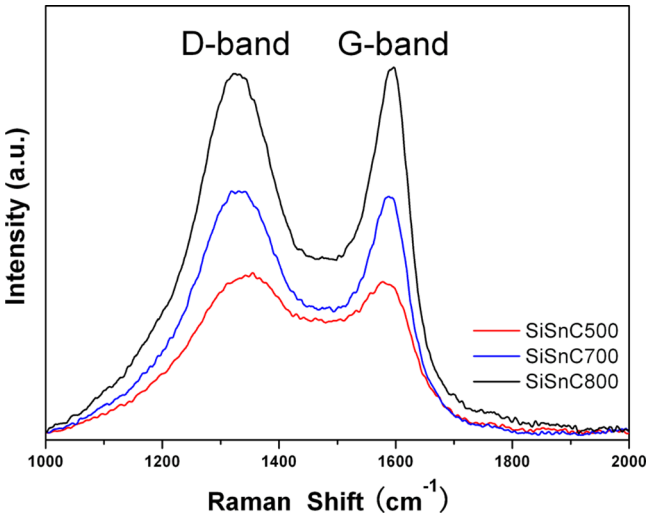

Figure 5. Raman spectra of SiSnC_500, SiSnC_700, and SiSnC_800.

almost reversible lithium alloying and dealloying of the as-synthesized Si/Sn/C composites is attributed to the buffering structure of carbon that hinders the aggregation of the nanoparticles or metal oxide enwrapped and dispersed in the carbon fibers. The relatively separated Si/Sn particles inside the carbon fibers are retained and none of the aggregation during charge/discharge, which demonstrates a good cycle performance. Compared with samples SiSnC_500 and SiSnC_700, the SiSnC_800 electrode has the highest capacities, which is probably due to two reasons: (i) The graphitization carbon fiber obtained at high temperature plays a major role in determining the discharge capacity, reversibility, and lithium extraction/reinsertion. As shown the above Raman spectra, SiSnC_800 has the lowest R value of 0.983 because the highest amount of sp^2 graphite exists. (ii) As shown XPS spectra, the relative intensity of the Si−C peak, Sn peak, and C−C peak increased with an increase in heat treatment temperature from 500 and 700 to 800 °C because the qualities of Si/Sn are increased instead of their oxides.

Figure 8 shows the profiles of differential discharge capacities of SiSnC_500, SiSnC_700, and SiSnC_800 at various cycles. The peaks in the first cycle disappeared, and those in the second cycle are always attributed to the irreversible processes. For all of the three samples, the reversible peaks observed between 0.08 and 0.3 V come from the reaction of Li ions with SiO_2 and Si. For sample SiSnC_500, a strong irreversible peak at 0.9 V corresponds to a reduction in Sn(IV) atoms and the formation of SEI film on the electrode. The peak centered at 0.35 V is attributed to the formation of lithium−tin alloys. For sample SiSnC_700, reversible peaks at 0.4 and 0.5 V suggest the reaction between Li and crystalline tin during electrochemical cycling. One irreversible peak at 1.12 V is located that is related to the catalytic decomposition of the electrolyte on the Sn surface. For sample SiSnC_800, two distinguishable

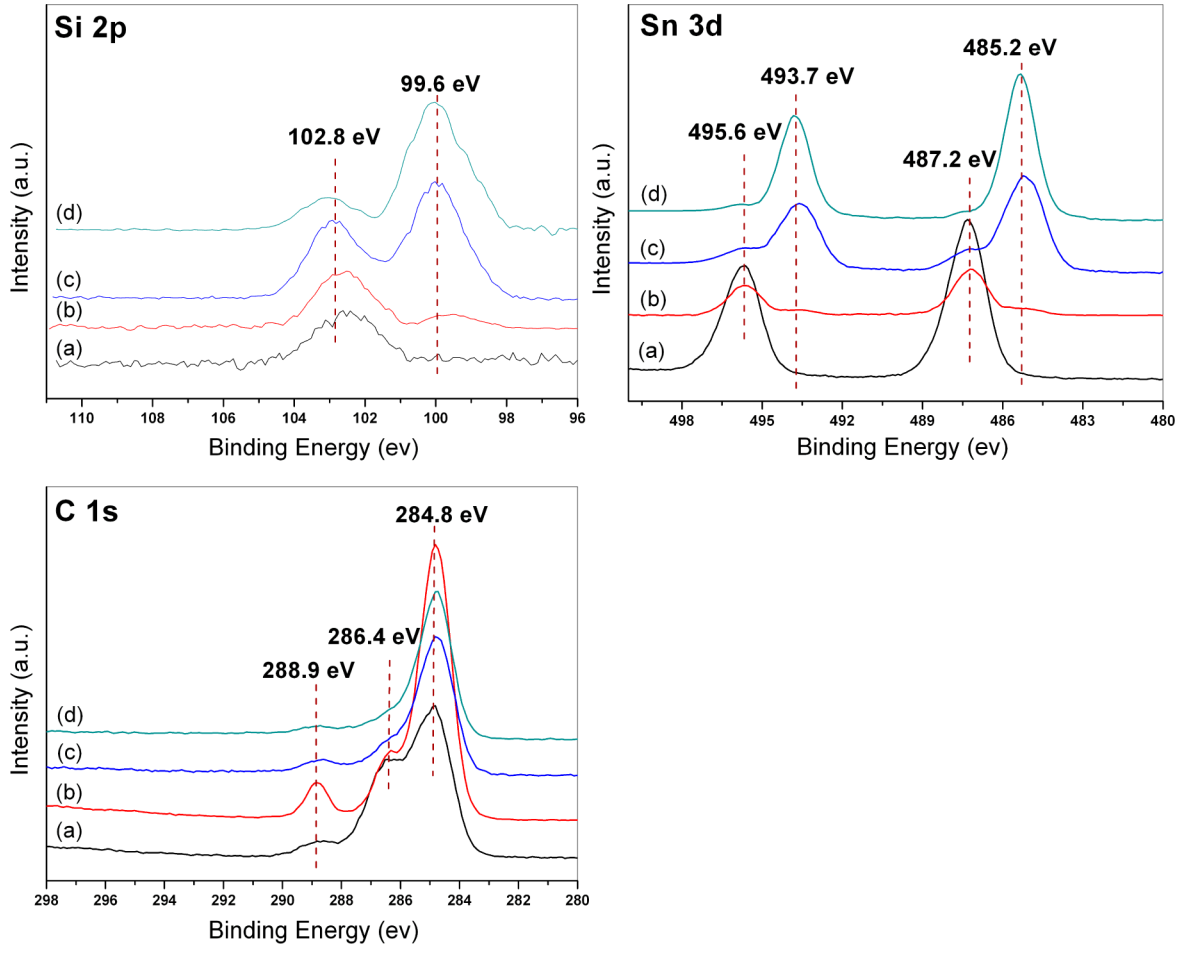

Figure 6. XPS spectra of (a) Si/Sn contained PAN film before heat treatment, (b) SiSnC_500, (c) SiSnC_700, and (d) SiSnC_800.

dx.doi.org/10.1021/sc500290x | ACS Sustainable Chem. Eng. 2014, 2, 2310−2317

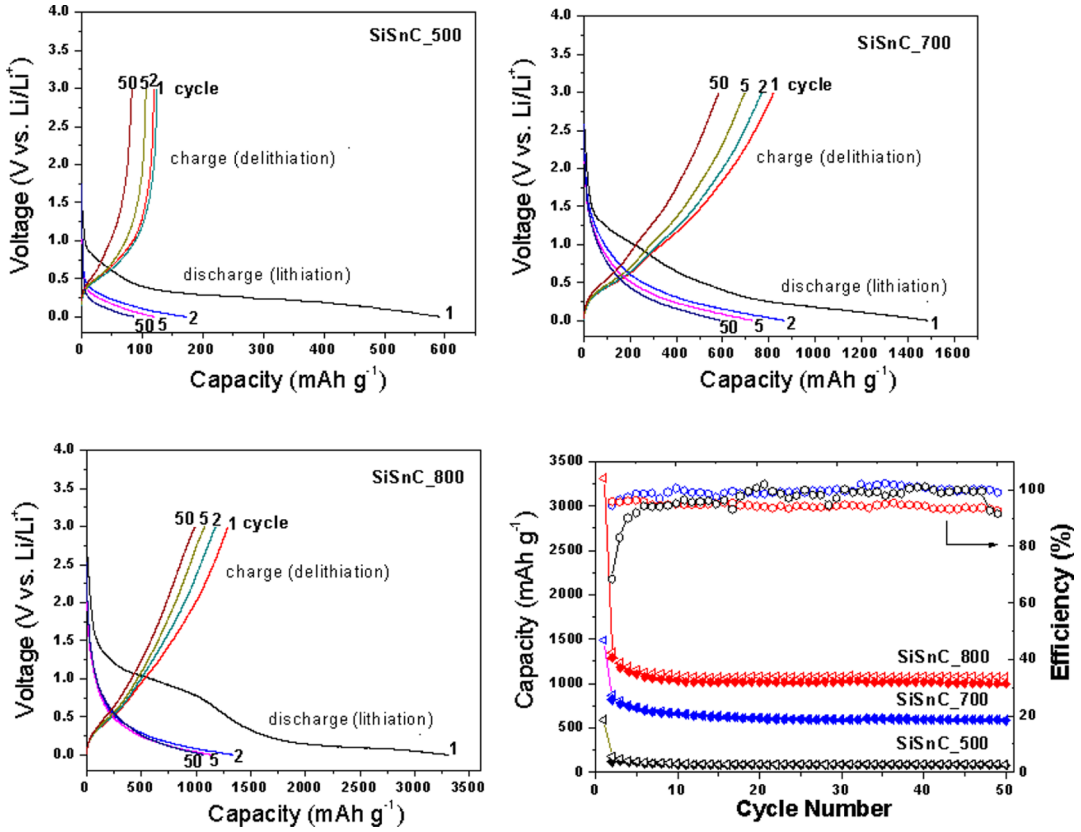

Figure 7. Charge/discharge profiles, cyclic performance, and columbic efficiency of SiSnC_500, SiSnC_700, and SiSnC_800.

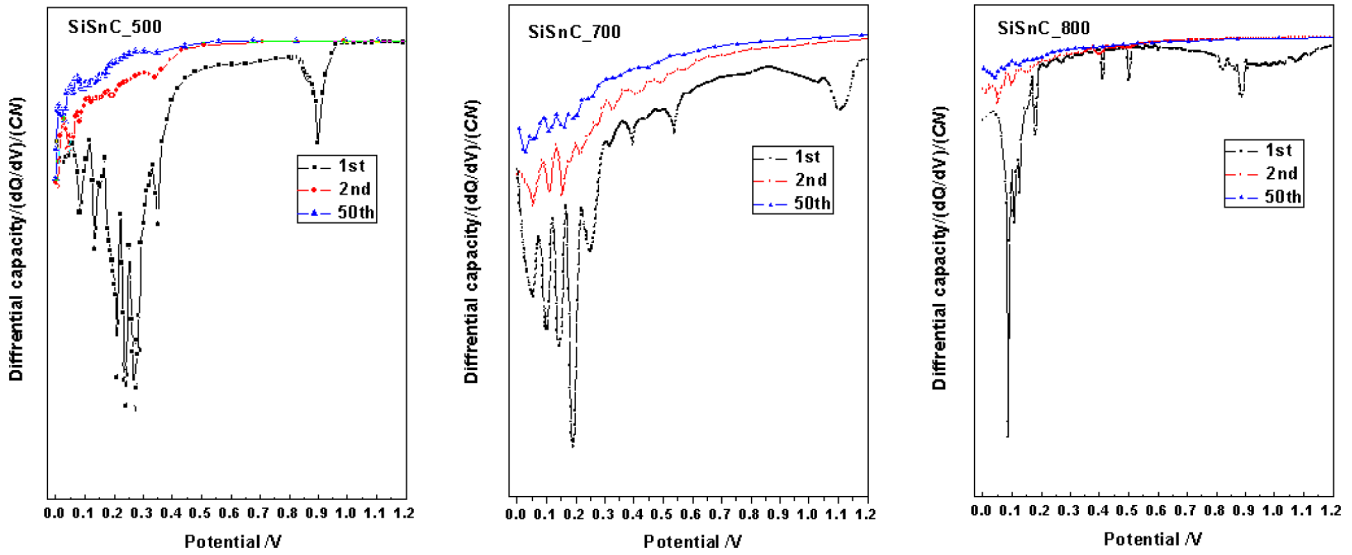

Figure 8. Evolution of differential discharge capacity plots of SiSnC_500, SiSnC_700, and SiSnC_800.

reversible peaks at around 0.4 and 0.5 V also correspond to the alloying reactions of Sn. Two irreversible peaks at 0.82 and 0.89 V are associated with electrolyte decomposition on the carbon surface. However, the irreversible peaks from the Sn components between 1.05 and 1.55 V are not found in sample SiSnC_800, implying that the Sn metal surface in the SiSnC_800 electrode is not exposed to the electrolyte. On the basis of the above results, the Si/Sn-based materials allocated in the carbon fiber are tunable, and the electrochemical performance is improved for the Si/Sn/C composites with proper composition and structure.

CONCLUSIONS

Through electrospinning, the precursors of TEOS/$SnCl_2$/PAN are synthesized. After thermal stabilization of the skeleton of PAN and carbonization, one-dimensional Si/Sn@C composites convert from TEOS/$SnCl_2$/PAN precursors. The Si/Sn nanoparticles are enwrapped and dispersed in carbon fibers. The crystal structure, composition, and morphologies of Si/Sn@carbon composites are tunable by the carbonization conditions. The electrochemical performance of the composites is improved by the buffer effect of carbon fibers. The sample of

dx.doi.org/10.1021/sc500290x | ACS Sustainable Chem. Eng. 2014, 2, 2310−2317

SiSnC_800 delivers a capacity of 1347 mAh g^{-1} in the second cycle and retains 1073 mAh g^{-1} after 50 cycles. The as-synthesized samples are flexible self-supporting films, which can be directly used as anode electrodes for lithium ion batteries. The synergetic effect among Si and Sn nanoparticles within carbon fibers plays a key role to enhance the electrochemical performance of the Si/Sn/C composite as an anode for lithium ion batteries.

AUTHOR INFORMATION

Corresponding Authors

*(G. Yang) E-mail: gyang@cslg.edu.cn. Tel: 86-512-52251895. Fax: 86-512-52251842.

*(Y. Yang) E-mail: yangyangirisjs@126.com.

Author Contributions

The manuscript was written through contributions of all authors. All authors have given approval to the final version of the manuscript.

Notes

The authors declare no competing financial interest.

ACKNOWLEDGMENTS

The work was supported by the Jiangsu Six-talent and Jiangsu "333" Project and NSF of China (Grants 51172032 and 51203013).

REFERENCES

(1) Goodenough, J. B.; Kim, Y. Selective crystallization with preferred lithium-ion storage capability of inorganic materials. *Chem. Mater.* **2010**, *22*, 587−603.

(2) Santhanam, R.; Rambabu, B. Research progress in high voltage spinel $LiNi_{0.5}Mn_{1.5}O_4$ material. *J. Power Sources* **2010**, *195*, 5442−5451.

(3) Whittingham, M. S. Lithium batteries and cathode materials. *Chem. Rev.* **2004**, *104*, 4271−4301.

(4) Zhang, W. J. A review of the electrochemical performance of alloy anodes for lithium-ion batteries Review article. *J. Power Sources* **2011**, *196*, 13−24.

(5) Aldon, L.; Garcia, A.; Olivier-Fourcade, J.; Jumas, J.-C.; Fernandez-Madrigal, F. J.; Lavela, P.; Vicente, C. P.; Tirado, J. L. Lithium insertion mechanism in Sb-based electrode materials from ^{121}Sb Mossbauer spectrometry. *J. Power Sources* **2003**, *119−121*, 585−590.

(6) Choi, N.-S.; Yao, Y.; Cui, Y.; Cho, J. One dimensional Si/Sn-based nanowires and nanotubes for lithium-ion energy storage materials. *J. Mater. Chem.* **2011**, *21*, 9825−9840.

(7) Hamon, Y.; Brousse, T.; Jousse, F.; Topart, P.; Buvat, P.; Schleich, D. M. Aluminum negative electrode in lithium ion batteries. *J. Power Sources* **2001**, *97−98*, 185−187.

(8) Shembel, E.; Apostolova, R.; Nagirny, V.; Kirsanova, I.; Grebenkin, P.; Lytvyn, P. Electrolytic molybdenum oxides in lithium batteries. *J. Solid State Electrochem.* **2005**, *9*, 96−105.

(9) Lin, Y. S.; Duh, J. G.; Shieh, D. T.; Yang, M. H. Effect of pH value on electrochemical property of tin compounds loaded graphite anodes for Li-ion battery applications. *J. Alloys Compd.* **2010**, *490*, 393−398.

(10) Beaulieu, L. Y.; Eberman, K. W.; Turner, R. L.; Krause, L. J.; Dahn, J. R. Colossal reversible volume changes in lithium alloys. *Electrochem. Solid-State Lett.* **2001**, *4*, A137−A140.

(11) Winter, M.; Besenhard, J. O. Electrochemical lithiation of tin and tin-based intermetallics and composites. *Electrochim. Acta* **1999**, *45*, 31−50.

(12) Grugeon, S.; Laruelle, S.; Herrera-Urbina, R.; Dupont, L.; Poizot, P.; Tarascon, J. M. Particle size effects on the electrochemical performance of copper oxides toward lithium. *J. Electrochem. Soc.* **2001**, *148*, A285−A292.

(13) Kang, H. K.; Lee, S. R.; Cho, W. I.; Cho, B. W. Effect of multilayer structure on cyclic performance of Si/Fe anodeelectrode in lithium-ion secondary batteries. *Phys. Chem. Chem. Phys.* **2013**, *15*, 1569−1577.

(14) Netz, A.; Huggins, R. A.; Weppner, W. The formation and properties of amorphous silicon as negative electrode reactant in lithium systems. *J. Power Sources* **2003**, *119−121*, 95−100.

(15) Wang, G. X.; Sun, L.; Bradhurst, D. H.; Zhong, S.; Dou, S. X.; Liu, H. K. Nanocrystalline NiSi alloy as an anode material for lithium-ion batteries. *J. Alloys Compd.* **2000**, *306*, 249−252.

(16) Weydanz, W. J.; Wohlfahrt-Mehrens, M.; Huggins, R. A. A room temperature study of the binary lithium−silicon and the ternary lithium−chromium−silicon system for use in rechargeable lithium batteries. *J. Power Sources* **1999**, *81−82*, 237−242.

(17) Wolfenstine, J. $CaSi_2$ as an anode for lithium-ion batteries. *J. Power Sources* **2003**, *124*, 241−245.

(18) Roberts, G. A.; Cairns, E. J.; Reimer, J. A. Magnesium silicide as a negative electrode material for lithium-ion batteries. *J. Power Sources* **2002**, *110*, 424−429.

(19) Tan, C. H.; Qi, G. W.; Li, Y. P.; Guo, J.; Wang, X.; Kong, D. L.; Wang, H. J.; Zhang, S. Y. The Improved performance of porous Sn−Ni alloy as anode materials for lithium-ion battery prepared by electrochemical dissolution treatment. *Int. J. Electrochem. Sci.* **2013**, *8*, 1966−1975.

(20) Yao, J. H.; Zhang, P. J.; Shen, C. Q.; Aguey-Zinsou, K.-F.; Wang, L. B. Three-dimensional macroporous Sn−Ag thin film anode prepared by electro-less reduction method: Effect of micro-structure. *Ionics* **2013**, *19*, 295−300.

(21) Guo, H.; Zhao, H.; Yin, C.; Qiu, W. Si/SnSb alloy composite as high capacity anode materials for Li-ion batteries. *J. Alloy. Compd.* **2006**, *426*, 277−280.

(22) Beaulieu, L. Y.; Hewitt, K. C.; Turner, R. L.; Bonakdarpour, A.; Abdo, A. A.; Christensen, L.; Eberman, K. W.; Krause, L. J.; Dahn, J. R. The electrochemical reaction of Li with amorphous Si−Sn alloys. *J. Electrochem. Soc.* **2003**, *150*, A149−A156.

(23) Beaulieu, L. Y.; Hatchard, T. D.; Bonakdarpour, A.; Fleischauer, M. D.; Dahn, J. R. Reaction of Li with alloy thin films studied by in situ AFM. *J. Electrochem. Soc.* **2003**, *150*, A1457−A1464.

(24) Suzuki, M.; Suzuki, J.; Sekine, K.; Takamura, T. Li insertion/extraction characteristics of a vacuum-deposited Si−Sn two-component film. *J. Power Sources* **2005**, *146*, 452−456.

(25) Dahn, J. R.; Mar, R. E.; Fleischauer, M. D.; Obrovac, M. N. The impact of the addition of rare earth elements to $Si_{1-x}Sn_x$ negative electrode materials for Li-ion batteries. *J. Electrochem. Soc.* **2006**, *153*, A1211−A1220.

(26) Hatchard, T. D.; Obrovac, M. N.; Dahn, J. R. A comparison of the reactions of the SiSn, SiAg, and SiZn binary systems with L3i. *J. Electrochem. Soc.* **2006**, *153*, A282−A287.

(27) Timmons, A.; Dahn, J. R. In situ optical observations of particle motion in alloy negative electrodes for Li-ion batteries. *J. Electrochem. Soc.* **2006**, *153*, A1206−A1210.

(28) Rock, N. L.; Kumta, P. N. Synthesis and characterization of electrochemically active graphite−silicon−tin composite anodes for Li-ion applications. *J. Power Sources* **2007**, *164*, 829−838.

(29) Wang, W.; Kumta, P. N. Nanostructured hybrid silicon/carbon nanotube heterostructures: Reversible high-capacity lithium-ion anodes. *ACS Nano* **2010**, *4*, 2233−2241.

(30) Wu, H.; Zheng, G. Y.; Liu, N.; Carney, T. J.; Yang, Y.; Cui, Y. Engineering empty space between Si nanoparticles for lithium-ion battery anodes. *Nano Lett.* **2012**, *12*, 904−909.

(31) Zhou, X. Y.; Tang, J. J.; Yang, J.; Xie, J.; Ma, L. L. Silicon@carbon hollow core−shell heterostructures novel anode materials for lithium ion batteries. *Electrochim. Acta* **2013**, *87*, 663−668.

(32) Jung, Y. S.; Lee, K. T.; Ryu, J. H.; Im, D.; Oh, S. M. Sn-carbon core-shell powder for anode in lithium secondary batteries. *J. Electrochem. Soc.* **2005**, *152*, A1452−A1457.

(33) Zou, L.; Gan, L.; Kang, F. Y.; Wang, M. X.; Shen, W. C.; Huang, Z. H. Sn/C non-woven film prepared by electrospinning as anode materials for lithium ion Batteries. *J. Power Sources* **2010**, *195*, 1216−1220.

(34) Li, D.; Xia, Y. N. Fabrication of titania nanofibers by electrospinning. *Nano Lett.* **2003**, *3*, 555−560.
(35) Ban, C. M.; Chernova, N. A.; Whittingham, M. S. Electrospun nano-vanadium pentoxide cathode. *Electrochem. Commun.* **2009**, *11*, 522−525.
(36) Wang, Y.; Ramos, I.; Aviles, J. J. S. Detection of moisture and methanol gas using a single electrospun tin oxide nanofiber. *IEEE Sens. J.* **2007**, *7*, 1347−1348.
(37) Yang, A.; Tao, F.; Pang, G. K. H.; Siu, K. G. G. Preparation of porous tin oxide nanobelts using the electrospinning technique. *J. Am. Ceram. Soc.* **2008**, *91*, 257−262.
(38) Yu, Y.; Gu, L.; Wang, C.; Dhanabalan, A.; Aken, P. A.; Maier, J. Encapsulation of Sn@carbon nanoparticles in bamboo-like hollow carbon nanofibers as an anode material in lithium-based batteries. *Angew. Chem., Int. Ed.* **2009**, *48*, 6485−6489.
(39) Wang, X. X.; Wang, J. N.; Chang, H.; Zhang, Y. F. Preparation of short carbon nanotubes and application as an electrode material in Li-ion batteries. *Adv. Funct. Mater.* **2007**, *17*, 3613−3618.
(40) Zussman, E.; Yarin, A. L.; Bazilevsky, A. V.; Avrahami, R.; Feldman, M. Electrospun polyaniline/poly(methyl methacrylate)-derived turbostratic carbon micro-/nanotubes. *Adv. Mater.* **2006**, *18*, 348−353.
(41) Yu, Y. H.; Yang, Q.; Teng, D. H.; Yang, X. P.; Ryu, S. Reticular Sn nanoparticle-dispersed PAN-based carbon nanofibers for anode material in rechargeable lithium-ion batteries. *Electrochem. Commun.* **2010**, *12*, 1187−1190.
(42) Yang, G.; Li, Y. H.; Ji, H. M.; Wang, H. Y.; Gao, P.; Wang, L.; Liu, H. D.; Pinto, J.; Jiang, X. F. Influence of Mn content on the morphology and improved electrochemical properties of Mn_3O_4| MnO@carbon nanofiber as anode material for lithium batteries. *J. Power Sources* **2012**, *216*, 353−362.
(43) Wang, H. Y.; Gao, P.; Lu, S. F.; Liu, H. D.; Yang, G.; Pinto, J.; Jiang, X. F. The effect of tin content to the morphology of Sn/carbon nanofiber and the electrochemical performance as anode material for lithium batteries. *Electrochim. Acta* **2011**, *58*, 44−51.
(44) Wang, Y.; Zeng, H. C.; Lee, J. Y. Highly reversible lithium storage in porous SnO_2 nanotubes with coaxially grown carbon nanotube overlayers. *Adv. Mater.* **2006**, *18*, 645−649.
(45) Timmons, A.; Todd, A. D. W.; Mead, S. D.; Carey, G. H.; Sanderson, R. J.; Mar, R. E.; Dahn, J. R. Studies of $Si_{1-x}C_x$ electrode materials prepared by high-energy mechanical milling and combinatorial sputter deposition. *J. Electrochem. Soc.* **2007**, *154*, A865−A874.
(46) Rahaman, M. S. A.; Ismail, A. F.; Mustafa, A. A review of heat treatment on polyacrylonitrile fiber. *Polym. Degrad. Stab.* **2007**, *92*, 1421−1432.
(47) Veeraraghavan, B.; Durairajan, A.; Haran, B.; Popov, B.; Guidotti, R. Study of Sn-coated graphite as anode material for secondary lithium-ion batteries. *J. Electrochem. Soc.* **2002**, *149* (6), A675−A681.
(48) Turner, R. L. World Intellectual Property Organization Patent Application WO 2000, 00/03444.
(49) Beaulieu, L. Y.; Eberman, K. W.; Turner, R. L.; Krause, L. J.; Dahn, J. R. Colossal reversible volume changes in lithium alloys. *Electrochem. Solid State Lett.* **2001**, *4*, A137−A140.
(50) Yang, Y.; Wang, H. Y.; Lu, X. F.; Zhao, Y. Y.; Li, X.; Wang, C. Electrospinning of carbon/CdS coaxial nanofibers with photoluminescence and conductive properties. *Mater. Sci. Eng., B* **2007**, *140*, 48−52.
(51) Lin, Z.; Ji, L.; Woodroof, M. D.; Yao, Y. F.; Krause, W.; Zhang, X. Synthesis and electrocatalysis of carbon nanofiber-supported platinum by 1-AP functionalization and polyol processing technique. *J. Phys. Chem. C* **2010**, *114*, 3791−3797.
(52) Nordberg, R.; Brecht, H.; Albridge, R. G.; Fahlman, A.; Van Wazer, J. R. Binding energy of the 2p electrons of silicon in various compounds. *Inorg. Chem.* **1970**, *9*, 2469−2474.
(53) Ding, W.; Li, L.; Zhang, L.; Ju, D.; Peng, S.; Chai, W. An XPS study on the chemical bond structure at the interface between SiO_xN_y and N doped polyethylene terephthalate. *J. Chem. Phys.* **2013**, *138*, 104706/1−104706/5.
(54) Yadav, J. B.; Patil, R. B.; Puri, R. K.; Puri, V. Studies on undoped SnO_2 thin film deposited by chemical reactive evaporation method. *Mater. Sci. Eng., B* **2007**, *139*, 69−73.
(55) Wang, Y.; Lee, J. Y.; Deivaraj, T. C. A microemulsion-based preparation of tin/tin oxide core/shell nanoparticles with particle size control. *J. Mater. Chem.* **2004**, *14*, 362−365.
(56) Huang, H.; Xia, Y.; Tao, X.; Du, J.; Fang, J.; Gan, Y.; Zhang, W. Highly efficient electrolytic exfoliation of graphite into graphene sheets based on Li ions intercalation−expansion−microexplosion mechanism. *J. Mater. Chem.* **2012**, *22*, 10452−10456.
(57) Yan, N.; Wang, F.; Zhong, H.; Li, Y.; Wang, Y.; Hu, L.; Chen, Q. W. Hollow porous SiO_2 nanocubes towards high-performance anodes for lithium-ion batteries. *Sci. Rep.* **2013**, *3*, 1568−1573.
(58) Menkin, S.; Golodnitsky, D.; Peled, E. Artificial solid-electrolyte interphase (SEI) for improved cycleability and safety of lithium-ion cells for EV applications. *Electrochem. Commun.* **2009**, *11*, 1789−1791.